Analyst

Accepted Manuscript

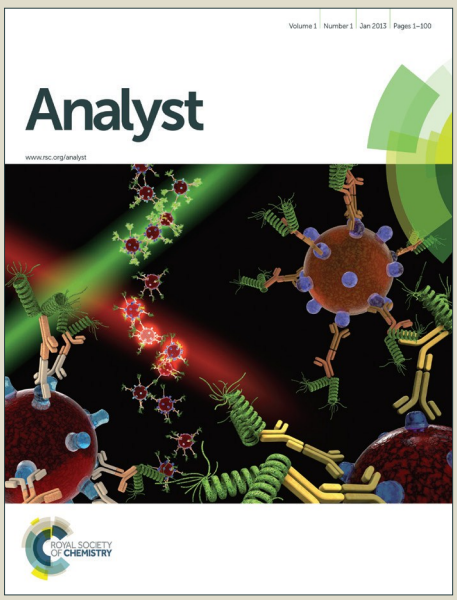

ROYAL SOCIETY OF CHEMISTRY

www.rsc.org/analyst

Microheterogeneity within Conformational States of Ubiquitin Revealed by High Resolution Trapped Ion Mobility Spectrometry

Mark E. Ridgeway, Joshua A. Silveira, Jacob E. Meier, and Melvin A. Park*

*Corresponding author

Author Affiliation:

Bruker Daltonics, 40 Manning Road, Billerica, Massachusetts, 01821, United States

Address Reprint Requests to:

Melvin A. Park

Bruker Daltonics, 40 Manning Road, Billerica, Massachusetts, 01821, United States

Phone: (978) 663-3600

E-mail: melvin.park@bruker.com

Journal: *Analyst*

Intended for the Themed issue on Ion mobility-Mass Spectrometry

Manuscript Type: *Full-length Research Article*

Keywords: trapped ion mobility spectrometry, mass spectrometry, ubiquitin, protein conformation, collision cross section, electrospray ionization, pseudopotential

ABSTRACT

The present work employs trapped ion mobility spectrometry (TIMS) for the analysis of ubiquitin ions known to display a multitude of previously unresolved interchangeable conformations upon electrospray ionization. The conformational distributions of ubiquitin $[M +6H]^{6+}$ through $[M + 13H]^{13+}$ ions observed by TIMS are nearly identical to numerous drift tube ion mobility spectrometry studies reported in the literature. At an experimental resolving power up to ~300, many of the congested conformations within the well-known compact, partially folded, and elongated $[M + 7H]^{7+}$ states are separated. Minimizing the voltages (RF and DC) in the entrance funnel results in exclusive observation of compact $[M + 7H]^{7+}$ conformers. However, under these conditions, the mobility-dependent pseudopotential coefficient may discriminate against ions having larger collision cross sections—a universal effect for all RF ion guides, funnels, and traps operating in the presence of a gas. The data presented underscore the complications associated with direct comparison of collision cross section values that represent an ensemble average of multiple underlying conformations. As illustrated herein, the microheterogeneity within a particular conformational family and the relative state-to-state abundance can be altered by solvent memory, energetic, and kinetic effects.

INTRODUCTION

Fundamental limitations associated with conventional bulk analysis methods (CD, NMR, X-ray crystallography, *etc*.) have led to the emergence of mass spectrometry (MS) as a complementary biochemical tool. One distinct advantage of MS is the ability to rapidly isolate and characterize individual components of a system in equilibrium. Of particular importance in the context of structural analysis is electrospray ionization (ESI) wherein desolvated analyte ions emerge directly from solution.[1,2] Though ions transition through various extents of solvation during the ESI process,[3-6] several studies have shown that ions produced by ESI can retain a memory of their solution conditions[7-11] and in some cases, major features of their solution structure up to seconds after desolvation.[12-18] Implicated in the preservation of native states are evaporative cooling leading to kinetic trapping on the experimental timescale,[4,5,19-25] the relative stability of the native fold,[26] and intramolecular interactions that stabilize dry ions after removal of remnant solvent from the charge sites.[5,22,27-29] In other cases, gaseous protein structures may be entirely different from their solution-phase counterparts because the global energy minimum in solution may only represent a local minimum in the gas phase.[30] In these cases, gentle instrument conditions that inhibit isomerization *via* energetic collisions are considered essential to the preservation of solution structures.[31]

To-date, one of the most well-studied protein systems in crystal, liquid, and gas phase is ubiquitin. Across a wide range of acidic and alkaline pH, NMR studies in aqueous solution found that ubiquitin adopts a compact native (N) state characterized by helical and β-sheet structural elements that persist in the presence of organic solvent and super-ambient temperatures.[32] In acidic solutions containing methanol in excess of 40%, a less compact form (A-state)—characterized by an N-terminal β-sheet domain and an extended C-terminal helical region—was observed, whereas an unstructured solution state has also been reported.[33] Early ion mobility spectrometry (IMS) studies by Clemmer and coworkers demonstrated that while high charge states (z > 8+) of ubiquitin ions exclusively adopt elongated gas phase structures, low charge states of ubiquitin (z < 8+) can adopt compact conformations upon ESI.[34,35] While the compact conformations are similar in size to the N-state and some of the elongated structures

are comparable in size to the A-state, many are not.[31,36] Compact states have been found to be stable in the gas phase on the timescale of drift tube IMS measurements (tens of ms); however, after storage in an ion trap for 40 ms, a significant increase in the collision cross section was observed, indicating substantial annealing had occurred.[37] Other experiments employing analyses with relatively longer timescales on the order of tens of milliseconds to seconds (*i.e.*: radical directed dissociation, and electron capture dissociation) also revealed evidence that low charge states of ubiquitin can adopt structures that do not resemble the N-state.[38,39]

Though it is widely accepted that ions in drift tube IMS operated below the "low-field limit" maintain temperatures near that of the thermal buffer gas,[40] other ion mobility techniques such as field asymmetric-waveform IMS[41] and ion mobility devices employing RF[42-44] can potentially heat ions *via* energetic collisions. Trapped ion mobility spectrometry (TIMS) is a new high resolution gas phase separation technique that inverts the traditional drift tube IMS experiment. Rather than forcing ions through a stationary gas with an electric field, an electric field is used to hold ions stationary against a moving gas. In TIMS, ions are radially trapped in a quadrupolar RF field and axially trapped by two opposing forces: a DC electric field gradient (EFG) that prevents ions from moving downstream and a flow of gas that prevents ions from moving upstream. After a packet of ions is accumulated in the tunnel, ions acquire an equilibrium position along the rising edge of the EFG. Ions are then eluted according to their mobility as the magnitude of the EFG is reduced.

Recently, Michelmann *et al.* derived a first-principles theory for TIMS that clarifies the dependence of instrument properties, user-defined experimental parameters, and ion characteristics on the analyzer performance.[45] In agreement with theory, we have demonstrated that for small peptides and model compounds, employing relatively slow EFG scans can yield resolving power exceeding 250.[46] In the present work, we test the reach of this approach for ubiquitin ions electrosprayed under "native-like" solution conditions known to yield compact (C), as well as numerous partially folded (P) and elongated (E) states that have been largely unresolved by conventional "high resolution" (R > 50) IMS methods.

Effects due to energetics, kinetics, and solvent memory are discussed in the context of numerous hybrid-MS studies of ubiquitin reported in the literature.

EXPERIMENTAL SECTION

Ubiquitin was prepared at a concentration of 1 μM in aqueous solutions containing 10-30% methanol and 0.1% formic acid; these solution conditions have previously been shown to produce compact conformers upon ESI.[47] Ubiquitin was also electrosprayed from denaturing solution conditions (50:50 water:acetonitrile containing 0.1% formic acid). In all cases, sample solutions were directly infused at a flow rate of ~150 μL/hr into a prototype ESI-TIMS-QqTOF mass spectrometer (Bruker Daltonics, Billerica, MA).

The details of the instrumentation have been previously described.[48-50] Briefly, the TIMS analyzer is comprised of three regions: an entrance funnel, tunnel (46 mm axial length), and exit funnel. An 850 kHz RF potential at variable peak-to-peak amplitude was applied to each section creating a dipolar field in the funnel regions and a quadrupolar field inside the tunnel. For all experiments, the ion accumulation time was 18 ms and the entrance funnel pressure of N_2 (g) was 3.8 mbar. Unless otherwise noted, the voltage scan rate (δ) was 142 V/s. Data were summed for 100 analysis cycles (938 ms/cycle) yielding analysis time on the order of 1.56 minutes/frame. Often a single frame is sufficient to measure narrow conformer distributions, though the broad distributions of 6+ and 7+ ions required ~5-10 frames for adequate sampling. For kinetics studies, ions were trapped in the analyzer for 2 to 350 ms before they are subsequently eluted by scanning the EFG. For collisional activation experiments, the peak-to-peak RF amplitude (V_{pp}) and axial field across the entrance funnel (V_f) were varied between 100-230 V_{pp} and 0-250 V_f. Reducing the peak-to-peak RF amplitude to 100 V_{pp} significantly decreased the ion intensities and required 50 analysis frames for sufficient sampling. Ion-nitrogen collision cross section values were determined by calibration of the elution voltage against the known reduced mobility values for low

concentration tuning mix ions (Agilent Technologies, Santa Clara, CA).[45,50] All resolving power (R) values reported herein were determined from Gaussian peak fits of the features in the TIMS distributions ($R = \Omega/\Delta\Omega$) using OriginPro (version 9.0).

For RF trapping studies, reserpine (*m/z* 609, Sigma Aldrich, St. Louis, MO) was added to low concentration tuning mix to yield a final concentration of 1 μg/mL. The peak monitored at *m/z* 663 is oxidized Naugard 524, a plasticizer commonly observed in its singly protonated form in ESI-mass spectra of tuning mix.[51] The mixture was analyzed by TIMS using an accumulation time of 7 ms and voltage scan rate of 695 V/s. Ion signals for each of the three analytes (*m/z* 609, *m/z* 622, and *m/z* 663) were measured as a function of the RF amplitude over the voltage range where ion transmission was first observed (100-210 V_{pp}).

RESULTS AND DISCUSSION

Charge State Dependent Ubiquitin Conformers. Figure 1a contains an ESI-mass spectrum of ubiquitin that shows a prominent distribution centered near the 8+ charge state and a secondary distribution centered near the 11+ charge state. Figure 1b contains TIMS distributions of *m/z*-selected $[M + zH]^{z+}$ (z = 6 to 13) ions with near-baseline separation of all major features comprising the 7+ to 13+ charge state dependent conformations. For comparison, discrete ion-nitrogen collision cross section values measured by drift tube IMS are shown as vertical lines. In agreement with other IMS experiments, protein ion conformations increase in size and often display less conformational heterogeneity as the charge state is increased.[52-54] Qualitatively, the conformer distributions for the 10+ to 13+ charge states are in excellent agreement with drift tube IMS studies recently reported by Bowers and coworkers.[31] There, the authors reported only a single population of 13+ ions whereas 10+ to 12+ ions were each comprised of two populations. Here, we observe a similar single major feature for 13+ ions and two discrete conformational families for 10+ to 12+ ions, though the higher resolving power afforded by

TIMS allows for partial separation of the conformations comprising each of the families. Very recently, von Helden and coworkers also reported two populations of 11+ ions separated by drift tube IMS.[55] UV photodissociation of each population revealed A-state-like gas phase conformations found to differ in the *cis/trans* orientation of a single peptide bond. Here, we clearly observe that the major feature in the bimodal distribution of 11+ ions contains at least two conformations. This result is consistent with the notion that many structurally similar isomers were present, but ultimately could not be resolved using drift tube IMS methods.

Table 1 shows a quantitative comparison of the ion-nitrogen collision cross section values measured by TIMS, and those measured by drift tube IMS. Owing to the conformational complexity of ubiquitin and the difference in resolving power between TIMS and drift tube IMS methods, evaluation of the data is not straightforward. It is clear from Figure 1 that the collision cross section values measured by TIMS generally agree with the literature values. However, exact comparison is complicated as it is unclear which conformations resolved by TIMS actually correspond to the discrete values previously reported. In the case of 8+, 9+, 12+, and 13+ ions, it appears that the major features contained in the TIMS distribution closely match the collision cross section of the literature values; however, in the case of 7+, 10+ and 11+ ions, assignment of the literature values to individual or collective features contained in the TIMS distribution is unclear. To semiquantitatively estimate the measurement agreement between the datasets, a weighted average collision cross section was calculated for 8+ to 13+ TIMS peaks having a relative abundance >10% within their respective distribution; note that these peaks are listed in Table 1. Comparison of the weighted average collision cross section value measured by TIMS and those reported in the literature yields good agreement; in ten of eleven measurements, the percent difference was < 1%. In one instance, the percent difference for 11+ ions was 3%. However, it appears that the particular conformer reported (2392 $Å^2$) was detected and accurately measured herein (2390 $Å^2$), though its abundance was only 28% relative to the conformer at 2300 $Å^2$. These data underscore the complications associated with direct comparison of collision cross section values that represent an ensemble average of

multiple underlying conformations. That is, only the peak centroid resulting from a conglomeration of conformations is measured with lower resolving power IMS techniques. As illustrated below, the microheterogeneity within a particular conformational family and the relative state-to-state abundance can be greatly altered by solvent memory, energetic, and kinetic effects.

z		Ω [Å^2]	Ω [Å^2] Weighted Average	Ω [Å^2] Ref. [56]	Ω [Å^2] Ref. [57]
7	N	1279			
	E_1	1760			
	E_2	1798			
	E_3	1816			
	E_4	1828			
	E_5	1841			
	E_6	1868		1910	
	E_7	1908			
	E_8	1933			
8		1970	1984		
		1988		1990	
9		2082	2092	2090	2080
		2110			
10		2159			
		2226	2206	2200	2228
		2244			
11		2300			
		2319	2319	2340	
		2390			2392
12		2460			
		2478	2476	2480	2473
		2560			
13		2637		2600	2625

Table 1. Comparison of the major features observed by TIMS and ion-nitrogen collision cross section values measured by drift tube IMS. For 8+ to 13+ ions, peaks with a relative abundance >10% within their respective distribution are listed, though several minor peaks were also observed (see Figure 1). Note that the $[M + 7H]^{7+}$ P state that spans ~1500 to 1750 Å^2 is omitted from the list.

Factors Affecting TIMS Distributions of $[M + 7H]^{7+}$ Ions. The data shown in Figure 2b-e demonstrate that as expected from TIMS theory, reducing the voltage scan rate by increasing the scan time results in superior resolving power. At a voltage scan rate of 122 V/s, at least eight prominent $[M + 7H]^{7+}$ elongated conformers are observed at a resolving power as high as ~300, though it is clear that several minor peaks are also present. However, increasing the measurement timescale also results in

changes in the conformer abundances comprising the family of $[M + 7H]^{7+}$ extended states such that the most abundant extended gas phase species (initially E_6) shifts toward E_2 (see discussion below).

Changes in the conformer abundances are also observed upon ESI from denaturing solvent conditions. As shown in Figure 2a, when electrosprayed from solvent containing acetonitrile, the most abundant conformer is E_2 while the abundances of E_1, E_4, and E_5 are significantly reduced. These results are consistent with observations made by Clemmer *et al.* wherein the relative abundance of the elongated states produced by collisional activation was dependent upon the solution condition from which the protein was electrosprayed.[58] These data have important implications when comparing collision cross section values across laboratories with IMS analyzers that yield lower resolving power—especially since only three of the conformers within the $[M + 7H]^{7+}$ elongated family have been resolved using drift tube IMS.[58] On the basis of relative peak positions in the TIMS measurements acquired at lower resolving power (Figure 2d-e), we speculate that the three elongated conformers previously observed in helium correspond to the peaks E_6, E_7, and E_8, whereas E_1 through E_5 are conformers that have not been previously resolved.

Of equal importance for structural studies of biomolecules in the gas phase are energetic effects that can alter the distribution of states. $[M + 7H]^{7+}$ ions provide a useful means to study energetic effects in TIMS because the conformers are known to exist in a diverse ensemble of compact, partially folded, and elongated conformations. The relatively high abundance of peaks P and E in the $[M + 7H]^{7+}$ distribution (see Figure 1b) indicates annealing has occurred prior to TIMS. Analogous to the effect of additional charge, weak activation has been shown to unfold a compact conformer into one of many partially folded states whereas stronger activation results in conversion into one of several elongated conformations.[34] Despite relatively large differences in collision cross section, von Helden *et al.* recently reported that many of the conformers comprising the P and E states yield near-identical UV photofragment ions, indicating that common structural motifs are shared and retained during the gas phase unfolding process.[59]

Here, the principal factors contributing to gas phase annealing prior to TIMS were expected to be: (1) the axial voltage across the entrance funnel, (2) the peak-to-peak amplitude of the RF voltage and (3) the measurement timescale. Figure 3 shows the effect of the first two variables dramatically alters the distribution of $[M + 7H]^{7+}$ ions observed. For example, applying 250 V_f across the entrance funnel and 230 V_{pp} RF, the $[M + 7H]^{7+}$ distribution is comprised almost entirely of population E; however, as both voltages are reduced, the relative abundance of peaks P and C significantly increase. Figure 4a shows that if both voltages are further minimized (0 V_f and 100 V_{pp}), it is possible to exclusively observe peak C and trap this ensemble of conformers for >250 ms in the gas phase without apparent changes in the peak width or observation of other states. Under these conditions, the observed signal intensities were significantly reduced. Alternatively, if the entrance funnel voltages are slightly increased (180 V_{pp} and 100 V_f, see Figure 4b), it is possible to simultaneously trap the C, P, and E states with only small changes over time to their respective abundances. Under the conditions described in Figure 4b, a small decrease in the abundance of peak C (~11% relative to peak P) was observed upon extending the trap time from 3 to 353 ms prior to elution of ions from the trap. This result is consistent with results from electron capture dissociation studies by Breuker *et al.* that found the native fold was unstable in the gas phase.[60] Moreover, because the relative abundance of conformer E_2 increased in each instance where the experimental timescale was increased (see Figures 2 and 4), it appears that this conformation is thermodynamically favored. Conversely, the concomitant decrease in E_6 (a presumed kinetically-favored conformer) clearly indicates that these conformers comprising the elongated states convert on the timescale of a few tens of milliseconds. Interestingly, tandem IMS experiments by Clemmer *et al.* determined that the conformers comprising peak C do not interconvert on a similar timescale.[61]

The data presented in Figures 3 and 4 demonstrate that the observation of gas phase structures (peaks P and E) is highly correlated with the entrance funnel potentials. One explanation is that structural conversions are inhibited at low voltages because the energy acquired by the ions between collisions is less than the energetic barriers required to transition between states—a hypothesis supported by previous

collisional activation tandem IMS experiments of conformer-selected $[M + 7H]^{7+}$ ions.[58] In this work, we also considered a secondary effect that, in part, can account for the absence of peaks P and E at low RF amplitudes. That is, partially folded and extended conformations are also presumably formed during the ESI process; however, these ions (having relatively larger Ω values at the same *m/z*) are discriminated against at low RF amplitudes because the radially-confining pseudopotential acting on them is preferentially dampened.

In a collisionally dampened regime, the mobility-dependent effective potential coefficient, γ, is given by,[62]

$$V_P^* = \gamma \cdot V_{vac}^* \quad [1]$$

$$\gamma = \frac{\omega^2\tau^2}{1+\omega^2\tau^2} \quad [2].$$

Here, V_P^* is the effective potential at a given pressure, V_{vac}^* is the effective potential in vacuum, and ω is the angular RF frequency. In eq. [2], the velocity relaxation time, τ, is expressed by,

$$\tau = \frac{Km}{ze} \quad [3]$$

where *K* is the ion mobility coefficient, *m* is the mass, *z* is the charge state, and *e* is the elementary charge. For $[M + 7H]^{7+}$ ubiquitin ions trapped under the experimental conditions used herein, the γ value for conformers occupying peak C (K_0 = 1.11 $cm^2 V^{-1} s^{-1}$) was found to be ~0.83 whereas γ for peak E_8 (K_0 = 0.732 $cm^2 V^{-1} s^{-1}$) was ~0.67. Thus, theory suggests that the radially-confining pseudopotential is ~1.2-fold greater for compact conformers, relative to the most elongated conformations of identical *m/z*. Though this difference appears small, it is difficult to independently assess the role of mobility-dependent collisional dampening directly from the data presented in Figures 3 and 4, since radial confinement effects cannot be decoupled from the known state-to-state transition processes.

We therefore measured ion transmission as a function of the RF amplitude during a TIMS experiment for a mixture of three structurally rigid ions of similar mass, having reduced mobility values that span a range near that of $[M + 7H]^{7+}$ ions (K_0 = 1.01 to 0.733 $cm^2 V^{-1} s^{-1}$; see experimental section for additional details). The data shown in Figure 5 indicate that the RF amplitude at which the onset of ion transmission occurs is strongly correlated with the collision cross section, consistent with equations [1-3]. The data also reveal that though the analytes were electrosprayed as a mixture, it is possible at a low RF amplitude (~150 V_{pp}) to selectively trap the ion having the smallest collision cross section, though the other two were also present in solution and were generated by ESI. The onset of ion transmission is not correlated to the relative ion intensities, which eliminates the possibility of threshold signal suppression. It is noteworthy that this outcome is not specific to TIMS but is a universal effect for all RF devices operating in the presence of a collision gas. In the context of ubiquitin, it now becomes somewhat unclear whether folded structures that arise from solution are simply preserved under gentle instrument conditions, or whether partially folded and elongated structures (that may also be transiently present in solution or produced during ESI) are suppressed at low RF amplitudes. Given that the axial voltage across the entrance funnel is not expected to strongly contribute to the preferential transmission of a particular mobility, it appears that collisional activation prior to TIMS still contributes to the presence of gas phase conformations, but that both effects can play a combined role in the distribution of states ultimately observed.

Resolving Power. The results presented above demonstrate that though several new peaks have been resolved for the elongated states of +7 to +13 ions, the compact and partially folded states of $[M + 7H]^{7+}$ ions (that are of principal interest for native MS studies) remained largely unresolved. Tandem IMS experiments have shown that peak C is comprised of many similar conformations that do not interconvert; in principle, these conformers could be resolved.[61] Here, it is obvious that peak C is considerably broader than expected for a single conformation. The ability to more easily differentiate conformers comprising the populations of extended states is not entirely due to greater structural heterogeneity of peak C. That is,

both theory and experiment have previously demonstrated that TIMS resolving power is mobility dependent, as R theoretically scales with $1/K^{3/4}$ (or $\Omega^{3/4}$).[45] Here, if we apply the known resolving power dependence across the entire mobility range, a resolving power of 295 at Ω = 1933 Å^2 translates into R ~216 at Ω = 1279 Å^2 making it inherently easier to separate ions having larger collision cross sections by TIMS.[45] This outcome also explains why in many cases, conformers of larger Ω within the partially-folded $[M + 7H]^{7+}$ family appear to be emerging from the ensemble, though individual features are not observed for peak C (see Figures 1 and 3).

It is noteworthy that while the $[M + 7H]^{7+}$ compact conformers are difficult to resolve, the TIMS distribution of $[M + 6H]^{6+}$ ions does indicate evidence for the emergence of features within the distribution of more compact ions (see Figure 1b). While the current resolving power of TIMS (R ~300) is significantly higher than alternative IMS techniques, the plurality of compact and partially folded conformations still requires higher resolving power to comprehensively characterize the vast conformational landscape of gas phase ubiquitin ions.

CONCLUSIONS

TIMS has been employed for conformational characterization of electrosprayed ubiquitin ions. Overall, the qualitative features and collision cross section values measured by TIMS were in excellent agreement with past drift tube IMS experiments. Consistent with several drift tube IMS studies, high charge states (z > 8+) exclusively displayed elongated structures, whereas $[M + 7H]^{7+}$ ions adopted a multitude of compact, partially folded, and elongated conformations. At a resolving power up to ~300, eight $[M + 7H]^{7+}$ prominent elongated conformers were observed in addition to several minor peaks. Many of the newly resolved $[M + 7H]^{7+}$ conformers appear to represent kinetically trapped species that transiently exist during the gas phase unfolding process.

Though the measurement timescale of TIMS (tens to hundreds of ms) can be longer than alternative IMS techniques, compact conformers were still readily observed. The relative abundance of the $[M + 7H]^{7+}$ C, P, and E states were found to be highly correlated to the potentials in the entrance funnel, indicating that gas phase annealing of protein ions can occur prior to TIMS. As expected from theory, a mobility-dependent pseudopotential dampening coefficient was found to suppress ions having the same *m/z* but larger collision cross sections when low RF amplitudes were employed—a universal effect for all RF devices that operate in the presence of a gas. The convolution of both effects—annealing and pseudopotential dampening—can play a role in the conformer distribution observed.

The high resolution capabilities of TIMS allow one to monitor the abundance of an individual conformation within a family as a function of timescale, energetics, and solution conditions. This ability should prove particularly useful in the context of structural analysis where more accurate collision cross section values can provide better constraints and improve structural assignments made from molecular dynamics simulations, spectroscopic signatures, and/or fragmentation techniques. Further improvement in TIMS resolving power is expected to reveal additional protein conformations—especially for compact conformers that are more closely related to the solution structure.

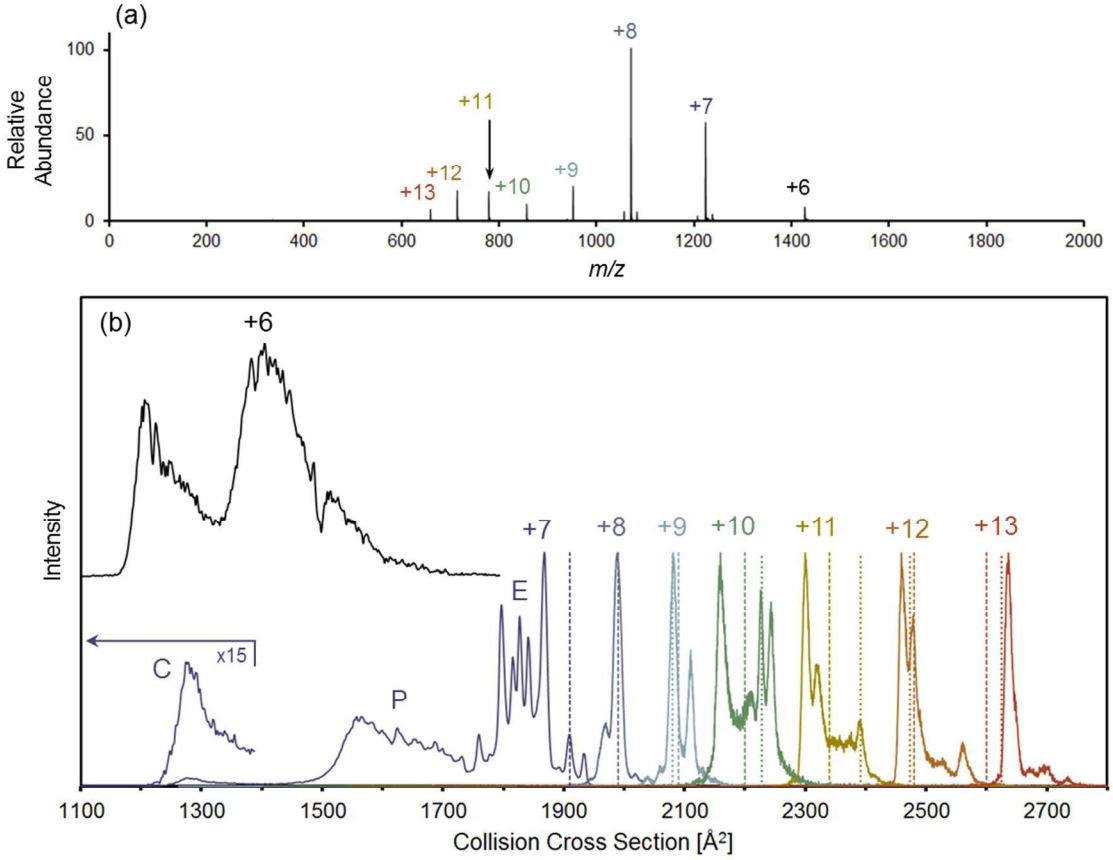

Figure 1. ESI-mass spectrum of ubiquitin (a) and mass-selected TIMS distribution of $[M + zH]^{z+}$ (z = 6 to 14) ions (b). For comparison, the dashed[56] and dotted[57] lines are collision cross section values from two independent datasets measured by drift tube IMS.

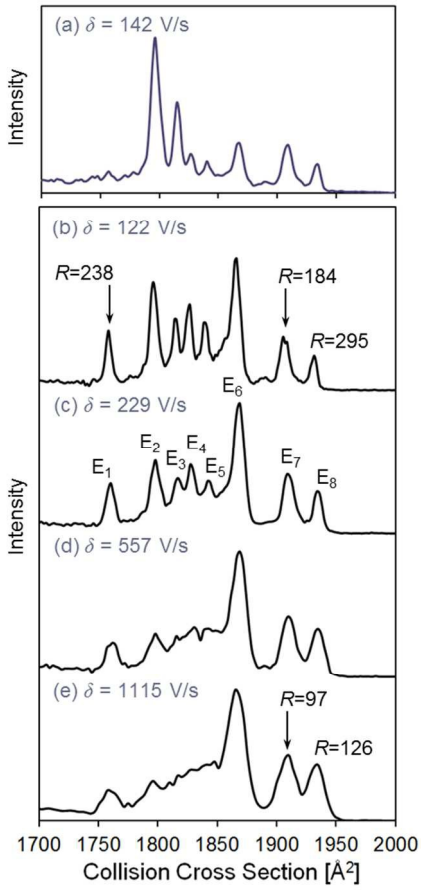

Figure 2. $[M + 7H]^{7+}$ elongated states observed upon electrospray ionization from denaturing (a) and "native-like" conditions (b-e, see experimental section for additional details). In (b-e), the voltage scan rate (δ) was decreased from 1115 to 122 V/s by increasing the scan time from 99 to 900 ms.

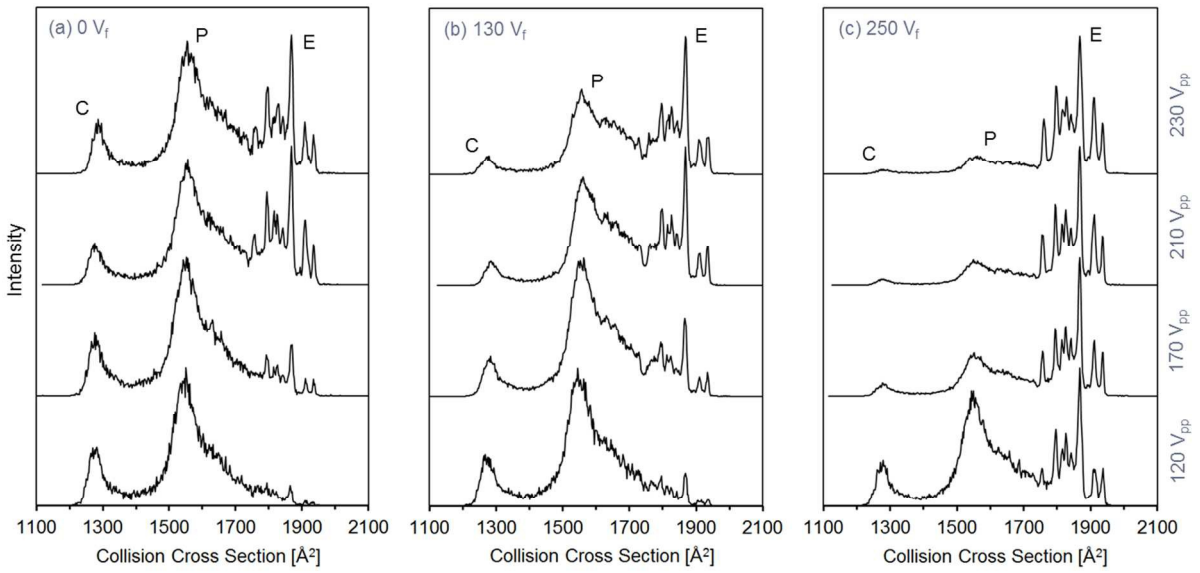

Figure 3. Distribution of compact, partially folded, and elongated $[M + 7H]^{7+}$ states observed as a function of the DC voltage applied across the entrance funnel (V_f) and peak-to-peak RF voltage amplitude (V_{pp}).

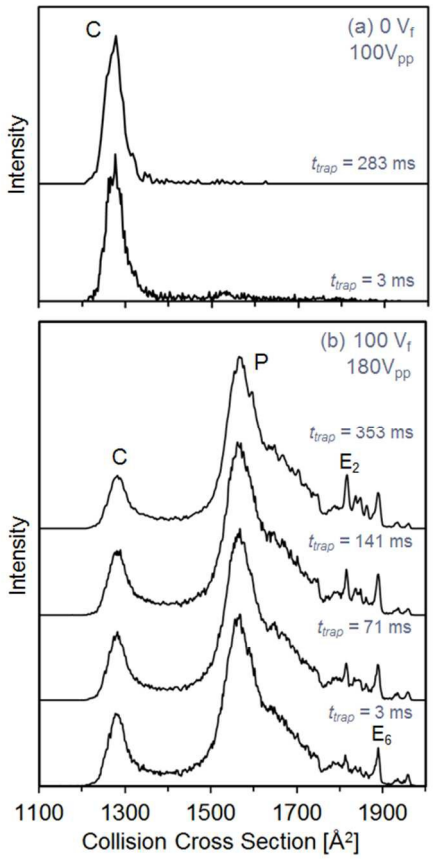

Figure 4. Distribution of compact, partially folded, and elongated $[M + 7H]^{7+}$ states observed as a function of the trap time, as indicated in each panel. The entrance funnel voltage (V_f) and peak-to-peak RF voltage (V_{pp}) were also varied in (a) and (b), as indicated in each legend.

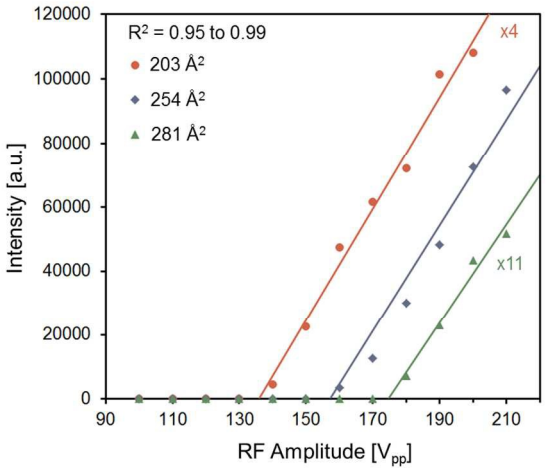

Figure 5. RF transmission curves during a TIMS experiment for singly charged ions of similar mass (● *m/z* 622, ♦ *m/z* 609, ▲ *m/z* 663) having differences in their collision cross sections. The solid lines are best-fit linear regression functions of the experimental data.

TOC Graphic

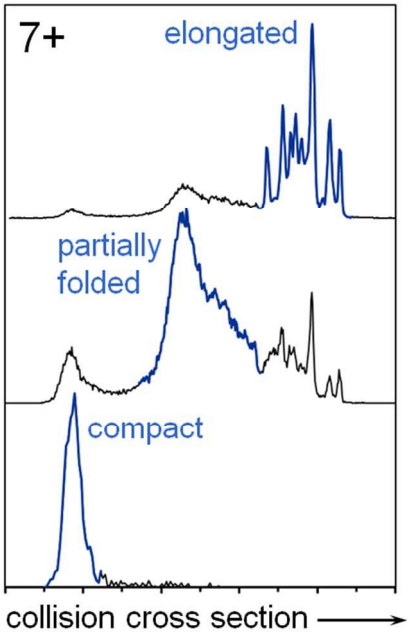

Reference List

1. Dole, M.; Hines, R. L.; Mack, L. L.; Mobley, R. C.; Ferguson, L. D.; Alice, M. B. Gas Phase Macroions. *Macromolecules* **1968,** *1* (1), 96-97.

2. Fenn, J. B.; Mann, M.; Meng, C. K.; Wong, S. F.; Whitehouse, C. M. Electrospray ionization for mass spectrometry of large biomolecules. *Science* **1989,** *246* (4926), 64-71.

3. Rodriguez-Cruz, S. E.; Klassen, J. S.; Williams, E. R. Hydration of Gas-Phase Gramicidin S (M + 2H)2+ Ions Formed by Electrospray: The Transition From Solution to Gas-Phase Structure. *Journal of the American Society for Mass Spectrometry* **1997,** *8* (5), 565-568.

4. Lee, S. W.; Freivogel, P.; Schindler, T.; Beauchamp, J. L. Freeze-Dried Biomolecules: FT-ICR Studies of the Specific Solvation of Functional Groups and Clathrate Formation Observed by the Slow Evaporation of Water from Hydrated Peptides and Model Compounds in the Gas Phase. *J. Am. Chem. Soc.* **1998,** *120* (45), 11758-11765.

5. Breuker, K.; McLafferty, F. W. Stepwise evolution of protein native structure with electrospray into the gas phase, 10-12 to 102 s. *Proc. Natl. Acad. Sci.* **2008,** *105* (47), 18145-18152.

6. Silveira, J. A.; Servage, K. A.; Gamage, C. M.; Russell, D. H. Cryogenic Ion Mobility-Mass Spectrometry Captures Hydrated Ions Produced During Electrospray Ionization. *J. Phys. Chem. A* **2013,** *117* (5), 953-961.

7. Pierson, N. A.; Chen, L.; Valentine, S. J.; Russell, D. H.; Clemmer, D. E. Number of Solution States of Bradykinin from Ion Mobility and Mass Spectrometry Measurements. *J. Am. Chem. Soc.* **2011,** *133* (35), 13810-13813.

8. Chen, L.; Chen, S. H.; Russell, D. H. An Experimental Study of the Solvent-Dependent Self-Assembly/Disassembly and Conformer Preferences of Gramicidin A. *Anal. Chem.* **2013,** *85* (16), 7826-7833.

9. Schenk, E. R.; Ridgeway, M. E.; Park, M. A.; Leng, F.; Fernandez-Lima, F. Isomerization Kinetics of AT Hook Decapeptide Solution Structures. *Anal. Chem.* **2013,** *86* (2), 1210-1214.

10. Shi, L.; Holliday, A. E.; Shi, H.; Zhu, F.; Ewing, M. A.; Russell, D. H.; Clemmer, D. E. Characterizing Intermediates Along the Transition from Polyproline I to Polyproline II Using Ion Mobility Spectrometry-Mass Spectrometry. *J. Am. Chem. Soc.* **2014,** *136* (36), 12702-12711.

11. Morrison, L. J.; Wysocki, V. H. Gas-Phase Helical Peptides Mimic Solution-Phase Behavior. *J. Am. Chem. Soc.* **2014,** *136* (40), 14173-14183.

12. Hofstadler, S. A.; Griffey, R. H. Analysis of Noncovalent Complexes of DNA and RNA by Mass Spectrometry. *Chem. Rev.* **2001,** *101* (2), 377-390.

13. Heck, A. J. R.; van den Heuvel, R. H. H. Investigation of intact protein complexes by mass spectrometry. *Mass Spectrom. Rev.* **2004,** *23* (5), 368-389.

14. Ruotolo, B. T.; Giles, K.; Campuzano, I.; Sandercock, A. M.; Bateman, R. H.; Robinson, C. V. Evidence for Macromolecular Protein Rings in the Absence of Bulk Water. *Science* **2005,** *310* (5754), 1658-1661.

15. Benesch, J. L.; Robinson, C. V. Mass spectrometry of macromolecular assemblies: preservation and dissociation. *Current Opinion in Structural Biology* **2006,** *16* (2), 245-251.

16. Barrera, N. P.; Di Bartolo, N.; Booth, P. J.; Robinson, C. V. Micelles Protect Membrane Complexes from Solution to Vacuum. *Science* **2008,** *321* (5886), 243-246.

17. Uetrecht, C.; Barbu, I. M.; Shoemaker, G. K.; van Duijn, E.; Heck, A. J. R. Interrogating viral capsid assembly with ion mobility–mass spectrometry. *Nat. Chem.* **2011,** *3* (2), 126-132.

18. Hall, Z.; Politis, A.; Bush, M. F.; Smith, L. J.; Robinson, C. V. Charge-State Dependent Compaction and Dissociation of Protein Complexes: Insights from Ion Mobility and Molecular Dynamics. *J. Am. Chem. Soc.* **2012,** *134* (7), 3429-3438.

19. Polfer, N. C.; Dunbar, R. C.; Oomens, J. Observation of Zwitterion Formation in the Gas-Phase H/D-Exchange with CH3OD: Solution-Phase Structures in the Gas Phase. *J. Am. Soc. Mass Spectrom.* **2007,** *18* (3), 512-516.

20. Schmidt, J.; Meyer, M. M.; Spector, I.; Kass, S. R. Infrared Multiphoton Dissociation Spectroscopy Study of Protonated p-Aminobenzoic Acid: Does Electrospray Ionization Afford the Amino- or Carboxy-Protonated Ion? *J. Phys. Chem. A* **2011,** *115* (26), 7625-7632.

21. Chang, T. M.; Prell, J. S.; Warrick, E. R.; Williams, E. R. Where's the Charge? Protonation Sites in Gaseous Ions Change with Hydration. *J. Am. Chem. Soc.* **2012,** *134* (38), 15805-15813.

22. Silveira, J. A.; Fort, K. L.; Kim, D.; Servage, K. A.; Pierson, N. A.; Clemmer, D. E.; Russell, D. H. From Solution to the Gas Phase: Stepwise Dehydration and Kinetic Trapping of Substance P Reveals the Origin of Peptide Conformations. *J. Am. Chem. Soc.* **2013,** *135* (51), 19147-19153.

23. Papadopoulos, G.; Svendsen, A.; Boyarkin, O.; Rizzo, T. Conformational Distribution of Bradykinin [bk+2H]2+ Revealed by Cold Ion Spectroscopy Coupled with FAIMS. *J. Am. Soc. Mass Spectrom.* **2012,** *23* (7), 1173-1181.

24. Inokuchi, Y.; Ebata, T.; Rizzo, T. R.; Boyarkin, O. V. Microhydration Effects on the Encapsulation of Potassium Ion by Dibenzo-18-Crown-6. *J. Am. Chem. Soc.* **2014,** *136* (5), 1815-1824.

25. Warnke, S.; Seo, J.; Boschmans, J.; Sobott, F.; Scrivens, J. H.; Bleiholder, C.; Bowers, M. T.; Gewinner, S.; Schollkopf, W.; Pagel, K.; von Helden, G. Protomers of Benzocaine: Solvent and Permittivity Dependence. *J. Am. Chem. Soc.* **2015,** *137* (12), 4236-4242.

26. Onuchic, J. N.; Socci, N. D.; Luthey-Schulten, Z.; Wolynes, P. G. Protein folding funnels: the nature of the transition state ensemble. *Folding and Design* **1996,** *1* (6), 441-450.

27. Liu, D.; Wyttenbach, T.; Barran, P. E.; Bowers, M. T. Sequential Hydration of Small Protonated Peptides. *J. Am. Chem. Soc.* **2003,** *125* (28), 8458-8464.

28. Fort, K. L.; Silveira, J. A.; Pierson, N. A.; Servage, K. A.; Clemmer, D. E.; Russell, D. H. From Solution to the Gas Phase: Factors That Influence Kinetic Trapping of Substance P in the Gas Phase. *J. Phys. Chem. B* **2014,** *118* (49), 14336-14344.

29. Servage, K. A.; Silveira, J. A.; Fort, K. L.; Russell, D. H. From Solution to Gas Phase: The Implications of Intramolecular Interactions on the Evaporative Dynamics of Substance P During Electrospray Ionization. *J. Phys. Chem. B* **2015,** *119* (13), 4693-4698.

30. Meyer, T.; Gabelica, V.; Grubmuller, H.; Orozco, M. Proteins in the gas phase. *WIREs Comput Mol Sci* **2013,** *3* (4), 408-425.

31. Wyttenbach, T.; Bowers, M. T. Structural Stability from Solution to the Gas Phase: Native Solution Structure of Ubiquitin Survives Analysis in a Solvent-Free Ion Mobility-Mass Spectrometry Environment. *J. Phys. Chem. B* **2011,** *115* (42), 12266-12275.

32. Vijay-Kumar, S.; Bugg, C. E.; Cook, W. J. Structure of ubiquitin refined at 1.8 A resolution. *J. Molec. Biol.* **1987,** *194* (3), 531-544.

33. Brutscher, B.; Bruschweiler, R.; Ernst, R. R. Backbone Dynamics and Structural Characterization of the Partially Folded A State of Ubiquitin by 1H, 13C, and 15N Nuclear Magnetic Resonance Spectroscopy. *Biochem.* **1997,** *36* (42), 13043-13053.

34. Koeniger, S. L.; Merenbloom, S. I.; Sevugarajan, S.; Clemmer, D. E. Transfer of Structural Elements from Compact to Extended States in Unsolvated Ubiquitin. *J. Am. Chem. Soc.* **2006,** *128* (35), 11713-11719.

35. Koeniger, S.; Clemmer, D. Resolution and structural transitions of elongated states of ubiquitin. *J. Am. Soc. Mass Spectrom.* **2007,** *18* (2), 322-331.

36. Shi, H.; Pierson, N. A.; Valentine, S. J.; Clemmer, D. E. Conformation Types of Ubiquitin [M+8H]8+ Ions from Water:Methanol Solutions: Evidence for the N and A States in Aqueous Solution. *J. Phys. Chem. B* **2012,** *116* (10), 3344-3352.

37. Myung, S.; Badman, E. R.; Lee, Y. J.; Clemmer, D. E. Structural Transitions of Electrosprayed Ubiquitin Ions Stored in an Ion Trap over ~10 ms to 30 s. *J. Phys. Chem. A* **2002,** *106* (42), 9976-9982.

38. Breuker, K.; Oh, H.; Horn, D. M.; Cerda, B. A.; McLafferty, F. W. Detailed Unfolding and Folding of Gaseous Ubiquitin Ions Characterized by Electron Capture Dissociation. *J. Am. Chem. Soc.* **2002,** *124* (22), 6407-6420.

39. Ly, T.; Julian, R. R. Elucidating the Tertiary Structure of Protein Ions in Vacuo with Site Specific Photoinitiated Radical Reactions. *J. Am. Chem. Soc.* **2010,** *132* (25), 8602-8609.

40. Mason, E. A.; McDaniel, E. W. *Transport Properties of Ions in Gasses;* John Wiley & Sons: New York, 1988.

41. Shvartsburg, A. A.; Smith, R. D. High-Resolution Differential Ion Mobility Spectrometry of a Protein. *Anal. Chem.* **2012,** *85* (1), 10-13.

42. Baker, E. S.; Clowers, B. H.; Li, F.; Tang, K.; Tolmachev, A. V.; Prior, D. C.; Belov, M. E.; Smith, R. D. Ion Mobility Spectrometry–Mass Spectrometry Performance Using Electrodynamic Ion Funnels and Elevated Drift Gas Pressures. *J. Am. Soc. Mass Spectrom.* **2007,** *18* (7), 1176-1187.

43. Morsa, D.; Gabelica, V. r.; De Pauw, E. Effective Temperature of Ions in Traveling Wave Ion Mobility Spectrometry. *Anal. Chem.* **2011,** *83* (14), 5775-5782.

44. Merenbloom, S.; Flick, T.; Williams, E. How Hot are Your Ions in TWAVE Ion Mobility Spectrometry? *J. Am. Soc. Mass Spectrom.* **2012,** *23* (3), 553-562.

45. Michelmann, K.; Silveira, J.; Ridgeway, M.; Park, M. Fundamentals of Trapped Ion Mobility Spectrometry. *J. Am. Soc. Mass Spectrom.* **2015,** *26* (1), 14-24.

46. Silveira, J. A.; Ridgeway, M. E.; Park, M. A. High Resolution Trapped Ion Mobility Spectrometery of Peptides. *Anal. Chem.* **2014,** *86* (12), 5624-5627.

47. Shi, H.; Clemmer, D. E. Evidence for Two New Solution States of Ubiquitin by IMS–IMS Analysis. *J. Phys. Chem. B* **2014,** *118* (13), 3498-3506.

48. Park, M. A. Apparatus and Method for Parallel Flow Ion Mobility Spectrometry Combined with Mass Spectrometry. US Patent 8,288,717, 2010.

49. Fernandez-Lima, F.; Kaplan, D. A.; Park, M. A. Integration of trapped ion mobility spectrometry with mass spectrometry. *Rev. Sci. Instrum.* **2011,** *82*, 126106.

50. Hernandez, D. R.; DeBord, J. D.; Ridgeway, M. E.; Kaplan, D. A.; Park, M. A.; Fernandez-Lima, F. Ion dynamics in a trapped ion mobility spectrometer. *Analyst* **2014,** *139*, 1913-1921.

51. Chen, S. W.; Her, G. R. Analysis of Additives in Polyethylene with Desorption Chemical Ionization/Tandem Mass Spectrometry. *Appl. Spectrosc.* **1993,** *47*, 844-851.

52. Clemmer, D. E.; Hudgins, R. R.; Jarrold, M. F. Naked Protein Conformations: Cytochrome c in the Gas Phase. *J. Am. Chem. Soc.* **1995,** *117* (40), 10141-10142.

53. Shelimov, K. B.; Clemmer, D. E.; Hudgins, R. R.; Jarrold, M. F. Protein Structure in Vacuo: Gas-Phase Conformations of BPTI and Cytochrome c. *J. Am. Chem. Soc.* **1997,** *119* (9), 2240-2248.

54. Sundarapandian, S.; May, J. C.; McLean, J. A. Dual Source Ion Mobility-Mass Spectrometer for Direct Comparison of Electrospray Ionization and MALDI Collision Cross Section Measurements. *Anal. Chem.* **2010,** *82* (8), 3247-3254.

55. Warnke, S.; Baldauf, C.; Bowers, M. T.; Pagel, K.; von Helden, G. Photodissociation of Conformer-Selected Ubiquitin Ions Reveals Site-Specific Cis/Trans Isomerization of Proline Peptide Bonds. *J. Am. Chem. Soc.* **2014,** *136* (29), 10308-10314.

56. Bush, M. F.; Hall, Z.; Giles, K.; Hoyes, J.; Robinson, C. V.; Ruotolo, B. T. Collision Cross Sections of Proteins and Their Complexes: A Calibration Framework and Database for Gas-Phase Structural Biology. *Anal. Chem.* **2010,** *82* (22), 9557-9565.

57. Kurulugama, R. T.; Mordehai, A.; Sanders, N.; Darland, E.; Klein, C.; Cody, C.; Barry, B.; Stafford, G. C.; Fjeldsted, J. C. Characterization of a New Uniform Field Ion Mobility Quadrupole Time of Flight Mass Spectrometer and its Application in Biomolecular Analyses. Conference Proceedings from the American Society for Mass Spectrometry. Baltimore, MD. 2015.

58. Shi, H.; Atlasevich, N.; Merenbloom, S.; Clemmer, D. Solution Dependence of the Collisional Activation of Ubiquitin [M + 7H]7+ Ions. *J. Am. Soc. Mass Spectrom.* **2014,** *25* (12), 2000-2008.

59. Warnke, S.; von Helden, G.; Pagel, K. Analyzing the higher order structure of proteins with conformer-selective ultraviolet photodissociation. *PROTEOMICS* **2015,** n/a.

60. Skinner, O. S.; McLafferty, F. W.; Breuker, K. How Ubiquitin Unfolds after Transfer into the Gas Phase. *J. Am. Soc. Mass Spectrom.* **2012,** *23* (6), 1011-1014.

61. Koeniger, S. L.; Merenbloom, S. I.; Clemmer, D. E. Evidence for Many Resolvable Structures within Conformation Types of Electrosprayed Ubiquitin Ions. *J. Phys. Chem. B* **2006,** *110* (13), 7017-7021.

62. Tolmachev, A. V.; Udseth, H. R.; Smith, R. D. Modeling the ion density distribution in collisional cooling RF multipole ion guides. *Int. J. Mass Spectrom.* **2003,** *222*, 155-174.